RADIATION RESEARCH **160**, 324–333 (2003)
0033-7587/03 $5.00
© 2003 by Radiation Research Society.
All rights of reproduction in any form reserved.

Comparative Microdosimetry of Photoelectrons and Compton Electrons: An Analysis in Terms of Generalized Proximity Functions

Albrecht M. Kellerer[a,b,1] and Jing Chen[c]

[a] *Radiobiological Institute, University of Munich, Germany;* [b] *Institute for Radiation Biology, GSF-National Research Center for Environment and Health, Germany; and* [c] *Radiation Protection Bureau 6302D1, Health Canada, Ottawa K1A 1C1, Canada*

Kellerer, A. M. and Chen, J. Comparative Microdosimetry of Photoelectrons and Compton Electrons: An Analysis in Terms of Generalized Proximity Functions. *Radiat. Res.* 160, 324–333 (2003).

A current discussion on mammography screening is focused on claims of high relative biological effectiveness (RBE) of mammography X rays compared to conventional 200 kV X rays. An earlier assessment in terms of the electron spectra of these radiations has led to the conclusion that the RBE is bound to be less than 2, regardless of specific model assumptions and the microdosimetric properties of electrons. The present study extends this result in terms of the microdosimetric *proximity function*, $t(x)$, for electrons, which is essentially the spatial auto-correlation function of energy within particle tracks. If pairs of DNA lesions, e.g. chromosome breaks or deletions, bring about the observed damage, the value $t(x)$ determines for a specified radiation the relative frequency of pairs of lesions a distance x apart. The effectiveness of the radiation is thus proportional to an average of the values of $t(x)$ over the distances, x, for which lesions can combine. The analysis suggests that 15 keV electrons can have a low-dose relative biological effectiveness (RBE_M) of 1.6 relative to 40 keV electrons if the interaction distances do not exceed about 1 μm. An extension of the concept, the *reduced proximity function*, $t_\Delta(x)$, permits the inclusion of models with an energy threshold, such as Δ = 100 eV, 500 eV or 2 keV, for the formation of each of the DNA lesions. This makes it possible to assess the potential impact of the Auger electrons which accompany most photoelectrons, but only a minority of the Compton electrons. It is found that the Auger electrons could make photoelectrons substantially more effective than Compton electrons at energies below 10 keV but not at energies above 15 keV. The conclusions obtained for the RBE of 15 keV electrons relative to 40 keV electrons will be roughly representative of the RBE of mammography X rays relative to conventional 200 kV X rays. © 2003 by Radiation Research Society

INTRODUCTION

A recent controversy (*1–5*) over claims of unexpectedly high relative biological effectiveness (RBE) of mammography X rays has generated increased interest in the relative biological effectiveness of different types of X rays. The current radiobiological evidence for a higher efficiency of soft X rays relative to conventional X rays is largely derived from the study of chromosome aberrations. Earlier experiments on the induction of dicentrics in human lymphocytes suggested little difference between 15 keV monoenergetic photons and 200 kV X rays (*6*). A more recent investigation (*7*) provides values for RBE_M of 1.6 ± 0.3 for 29 kV X rays relative to moderately filtered 200 kV X rays and 3.0 ± 0.7 relative to strongly filtered 200 kV X rays.

The familiar interpretation assumes the relative biological effectiveness at low dose (RBE_M) to be proportional to the dose-averaged *linear energy transfer*, $L_{\Delta,D}$, of the radiation or its microdosimetric analogue, the dose mean *lineal energy*, y_D, or *specific energy*, z_D. With this assumption there should be little difference in RBE_M within the energy range of X rays that is relevant to medical diagnostics, i.e. between 30 kV mammography X rays and conventional X rays of, say, 200 kV with normal filtration (*3, 4, 8*). However, it has been argued (*2, 9*) that the range of the photoelectrons released by soft X rays might be a critical factor not reflected in the LET values.

In response to these considerations, an assessment has been made of the energy spectra of electrons released by mammography X rays and 200 kV X rays (*3*). Under the plausible ''monotony'' assumption that an electron of higher energy has no less effect than one of lower energy, it was deduced that the RBE_M of the mammography X rays must be less than 2. The strength of the argument is its simplicity and its reference to the actual X-ray spectra. But it provides an upper bound only and not a point estimate of RBE_M. Also, the ''monotony'' assumption is not entirely rigorous, since it disregards the fact that all photoelectrons—but only 20% of the Compton electrons—are accompanied (in water) by a 0.5 keV Auger electron. The ''combined'' tracks of the photoelectrons have a densely ionizing 0.5 keV ''track end'' not only at their terminal point but also at their starting point. They thus might be somewhat more likely to create adjacent chromosomal lesions than Compton electrons of the same total energy.

[1] Address for correspondence: Radiobiological Institute, University of Munich, Schillerstr. 42, D-80336 Munich; e-mail: amk.sbi@lrz.uni-muenchen.de.

The exploration of the potential impact of the Auger electron was outside the scope of the preceding analysis and was judged unlikely to affect the conclusions in a major way (*3*). It is nevertheless of interest to examine the microdosimetry of photoelectrons and Compton electrons. This is done here in terms of a treatment that provides a flexible method to assess the potential RBE_M of different types of photon radiation.

THE PROXIMITY FUNCTION

The principal tool in the subsequent analysis is the microdosimetric concept of the *proximity function, t*(*x*). It is essentially the spatial auto-correlation function of energy transfers within charged-particle tracks; i.e., it characterizes radiation quality by specifying the distribution of distances, *x,* between energy transfers in the particle track. The proximity function is well suited to quantify the RBE_M of photon radiations under models where two energy deposits a small distance apart can create pairs of lesions,[2] e.g. two chromosome breaks or two chromosomal deletions, which then combine and produce the observed effect (*10, 11*). The concept has been variously applied for the analysis of radiobiological studies. Recent applications were directed at the determination of RBE for treatment planning in brachytherapy (*12, 13*), and—in another approach that is of particular interest—the proximity function has been applied to radiochemistry (*14*). Although the concept is known, it will be explained here in its essentials to facilitate the presentation.

The Concept of Energy Transfers

An electron track, as that of any charged ionizing particle, consists of *transfer points,* t_i (*10, 11, 15, 16*). These are the points where the electron or one of its secondaries loses some or all of its kinetic energy. The energy loss, i.e. the difference between the kinetic energy of the incoming electron and the sum of the kinetic energies of the emerging electron(s), is termed the *energy transfer,* ε_i, at the point. Electrons below a specified *energy cut-off,* Δ, are not followed further, i.e. the energy, Δ, of the *track ends* is taken to be absorbed locally.

In track simulations, the cut-off energy, Δ, is usually taken to be equal to the minimum kinetic energy required to produce an ionization in tissue-equivalent gas or in water. The standard value in the subsequent computations is $\Delta = 12.6$ eV. However, substantially larger values of Δ will also be considered in addition to explore models where the observed effect is due to pairs of lesions that are formed with an energy threshold, Δ. The value $\Delta = 100$ eV is considered in line with conclusions from ultrasoft X-ray experiments (*17–19*). The larger values 0.5 keV and 2 keV are less plausible, but they will serve to explore the maximum conceivable impact of the Auger electrons.

[2] The term ''lesion'' is used for each of the two defects that can combine or interact to bring about the observable damage. There is no fixed convention on the terminology. What is here called *lesion* is in part of the literature termed *sublesion.*

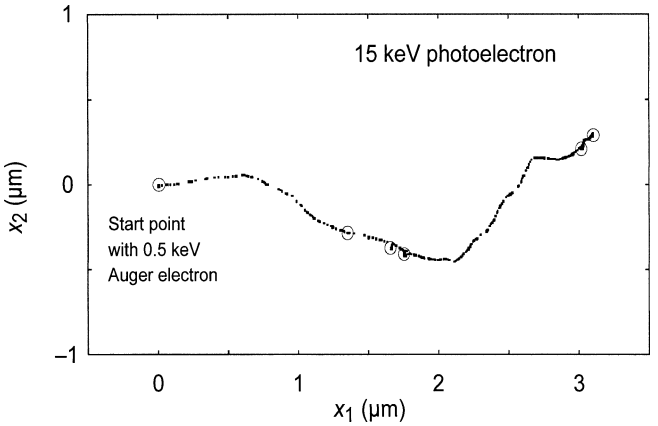

FIG. 1. Planar projection of a simulated 15 keV combined electron track, i.e. a 14.5 keV electron accompanied by a 0.5 keV Auger electron. The track starts out in the x_1 direction. The proximity function, i.e. the point-pair distance distribution, for 15 keV electrons is given in Fig. 2. Light dots: energy transfers; circles: 0.5 keV track ends.

Figure 1 gives the planar projection of a simulated 15 keV photoelectron track. Each small dot represents a transfer point. The circles mark the 0.5 keV electron track ends. The circle at the origin represents the 0.5 keV Auger electron from oxygen that accompanies the photoelectron.

Definition of the Proximity Function

The proximity function, $t(x)$, is defined (*10, 11, 16*) as the weighted distribution of distances between energy transfers on a charged-particle track. The concept is applicable to all types of ionizing radiation, but only electrons of specified initial energy, *E,* are considered here. Since $t(x)\,dx$ equals the expected sum of energy transfers within distance x to $x + dx$ from a randomly chosen transfer, the distribution $t(x)$ is normalized to *E.*

For the derivation of the results in Fig. 2 and of the subsequent data consider an electron track with transfer points t_i ($i = 1, 2, \ldots I$) and energy transfers ε_i. The *integral proximity function* of the track is then

$$T(x) = \sum_{k,i} \varepsilon_k \varepsilon_i / E$$

(summation over all i and k with $s_{i,k} \leq x$);

$s_{i,k}$: distance between the transfer points t_i and t_k;

E: energy of particle track. (1)

In actuality $T(x)$ is the average over a large number of tracks. The integral proximity function equals the expected sum of energy transfers on the particle track at distances up to x from randomly selected energy transfers.

The (*differential*) *proximity function* is the derivative of $T(x)$:

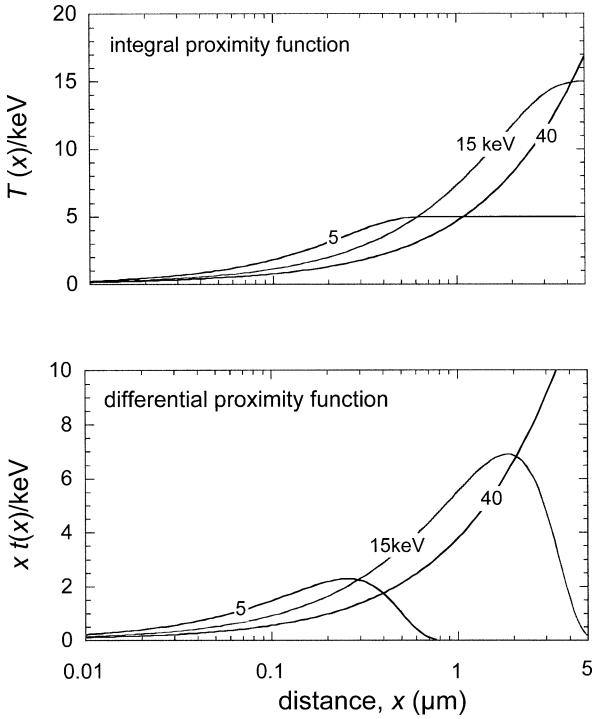

FIG. 2. Integral and differential proximity functions for electrons of 5, 15 and 40 keV. In the lower panel, the factor x relates the distributions to the logarithmic scale in distance.

$$t(x) = \mathrm{d}T(x)/\mathrm{d}x. \tag{2}$$

Applicability of t(x) in Radiobiology

As stated in the Introduction, it is of interest to explore models which have been invoked (*2, 9*) to explain a high effectiveness of electrons of about 15 keV. These electrons are roughly representative of the X rays used in mammography. They have somewhat elevated LET, but their range is still comparable to interchromosomal distances. 40 keV Compton electrons can roughly represent conventional 200 kV X rays.

Figure 2 gives for illustration the integral and the differential proximity functions for 5, 15 and 40 keV electrons. Since a wide range of distances is considered, a logarithmic scale is chosen for x. The term $T(x)$ gives the expected energy deposited by the same electron within distance x from a randomly chosen energy transfer point. $t(x)$ gives the corresponding differential distribution of energy imparted in distance. The scaling factor, x, is used to relate the differential distributions to the log-scale of x. The area under the function x t(x) remains then equal to the energy of the particles, i.e. 5, 15 and 40 keV.

The input data to the calculations are simulated tracks generated by the Monte Carlo code of electron transport in water described by Zaider *et al.* (*20*), with some modifications of the cross sections as used by Kellerer *et al.* (*21*). In the calculations, a code modification is employed to include four main Auger electron lines from oxygen (*22*) as indicated by Chen *et al.* (*23*).

As stated, the concept of the proximity function is useful for treating models where two lesions in a cell, e.g. two chromosome breaks or two deletions, can bring about the effect. A comprehensive survey of radiobiological applications is found in the monograph on microdosimetry by Rossi and Zaider (*11*). However, the essential idea can be readily understood even without mathematical formalism.

The function $T(x)$ specifies for a lesion the expected energy imparted within distance x by the same particle track. Accordingly it also specifies the frequency of neighboring lesions, i.e. of potential reaction partners. Figure 2 shows that for an energy transfer on a 15 keV track, there is on average 7.3 keV energy imparted by the same particle within the associated sphere of radius 1 μm; for an energy deposit on the somewhat less densely ionizing 40 keV track, the value is only 4.6 keV; i.e., it is less by a factor of 1.6. If lesions can combine up to about 1 μm, the 15 keV electrons should thus have an RBE_M of 1.6 relative to the 40 keV electrons. The differential distribution permits a more detailed distance-dependent argumentation, but it carries essentially the same information. Within the usual approach, where the yield of the lesions themselves is not taken to be dependent on radiation quality, the answer would thus be clear and there would be little need for further analysis.

However, there is no assurance that the yield of lesions is independent of radiation quality, and a major change in the analysis is therefore required. It will be seen that this change can be achieved by a rather straightforward extension of the concept of the proximity function.

CONSIDERATION OF AN ENERGY THRESHOLD FOR LESION PRODUCTION

Need to Consider a Threshold

Earlier "*dual action*" microdosimetric models (*24–26*) were applied to various radiobiological studies with neutrons. They were patterned after classical two-lesion interaction models (*27, 28*), and no threshold was assumed for creating a lesion in a target; i.e., chromosomal target structures were taken to react with probability proportional to the energy imparted.

In subsequent studies with ultrasoft X rays, Cox, Thacker and Goodhead (*17–19*) concluded that a single lesion was sufficient to induce the inactivation or mutation of a mammalian cell. With reference to chromosome aberrations one would speak of a *lesion–non-lesion* interaction with threshold Δ. With reference to microdosimetric data, Goodhead and Brenner inferred a threshold of about $\Delta = 100$ eV in a site of 3 nm for producing a lesion (*19*). The authors noted that the same threshold assumption may need to be incorporated into *two-lesion* interaction models.

In view of these considerations, it must be asked whether an RBE_M larger than 2 or 3 can be explained either by a

single lesion model with threshold or by a two-lesion model with threshold. While the experiments with ultrasoft X rays suggest a threshold of $\Delta = 100$ eV, higher threshold values, 0.5 keV and even 2 keV, will be likewise considered to explore models that might tentatively be invoked to explain a high RBE of photons in the range of 10 keV to 20 keV.

Photoelectron and Compton Electron

A photoelectron and a Compton electron of the same total energy, *E*, are somewhat different entities. A photoelectron is usually accompanied by an Auger electron. In water, the energy of the photoelectron, *E*, is 0.5 keV, while 0.5 keV is the energy of the associated Auger electron from oxygen. The two electrons originate from the same point in uncorrelated directions and they are here treated as one *combined track.* The same process occurs for only two of the 10 Compton electrons from the oxygen K shell; the remaining eight are Compton electrons with initial energy *E*. In tissue there are also some more energetic photon-induced Auger electrons at the starting point of photoelectrons. The present calculations use the photoelectric ionization cross sections for the elements potassium, sulfur, phosphorus and chlorine in tissue (*29, 30*). This results, for photon energies of 15 keV to 40 keV, in 7% of the initial photon-induced Auger electrons having an energy of about 2 keV, while 8% have about 3 keV. The remainder are the 0.5 keV oxygen Auger electrons. The higher-energy Auger electrons are essential with regard to a speculative ''2 keV threshold model'' where a high 2 keV threshold is contemplated for the production of chromosomal deletions (*31, 32*) and two deletions are assumed to cause neoplastic transformation (*2, 33*).

To keep the terminology as simple as possible, the electrons with an Auger electron are subsequently called photoelectrons, and the electron energy is stated as the sum of the two electron energies. The electrons without an Auger electron are termed Compton electrons. This disregards the fact that a minority of the Compton electrons are equally accompanied by an Auger electron, but use of the more appropriate terms *combined track* and *plain track* would complicate the terminology and make the presentation less transparent.

The Compton electron has somewhat lower dose-averaged LET than the photoelectron of the same (total) energy. However, the overall difference is not large. In terms of average LET there is thus no reason to expect the photoelectrons to be considerably more efficient than the Compton electrons (*2*). But when a threshold for lesion induction is considered, only those parts of the particle track matter where high local energy densities occur, and the additional Auger electron could then make a substantial difference.

Number of Track Ends

With electrons it is justified to assume that only through the track ends (including those of the more energetic δ rays) a threshold energy, Δ, is imparted to a small target. The track ends are accordingly the critical events in the threshold model.[3]

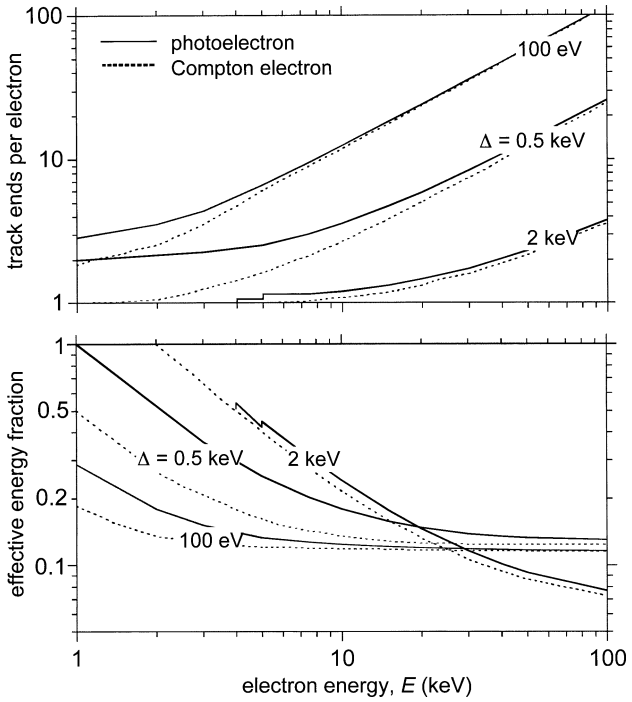

FIG. 3. Upper panel: The mean number per electron of track ends of specified energy Δ. Lower panel: The effective energy fraction, i.e. the fraction of energy in track ends. Solid curves: photoelectrons; broken curves: Compton electrons (no initial Auger electron).

Each photoelectron of energy larger than 2Δ has—as part of its associated Auger electron—an additional track end at its origin. For higher electron energies there will be further track ends per electron as part of the more energetic δ rays. For example, a 15 keV photoelectron has on average 18.2 track ends of 100 eV, but only 4.7 track ends of 500 eV (i.e. 1.3 less than the sample track in Fig. 1).

The upper panel in Fig. 3 gives—based on the simulations—the expected numbers, $n_\Delta(E)$, of track ends for Compton and photoelectrons of starting energy up to 100 keV. The lower panel in Fig. 3 gives the corresponding, more tangible parameter *effective energy fraction* for $\Delta =$ 100 eV, 0.5 keV and 2 keV:

$$f_\Delta(E) = n_\Delta(E)\Delta/E. \tag{3}$$

The solid curves refer to photoelectrons, the broken curves to Compton electrons (without initial Auger electron).

RBE_M Values for the Single-Lesion Model with Threshold

With the single-lesion model (*lesion–non-lesion interaction*) and an assumed threshold, Δ, the RBE_M is simply

[3] A corresponding assumption will not be justified for densely ionizing heavy particles, because threshold energies Δ can then be imparted to a small target by coincidence of several closely spaced δ rays. The mean number of track ends is termed *multiplication factor* in the Spencer-Fano theory of electron slowing down (*34, 35*).

proportional to the effective energy fraction. The data in the lower panel of Fig. 3 then provide for 15 keV photoelectrons relative to 40 keV Compton electrons the values RBE_M = 1.05, 1.27 and 1.89 for the assumed threshold values Δ = 100 eV, 0.5 keV and 2 keV. The 2 keV threshold model is, of course, not consistent with the high effectiveness of ultrasoft X rays. But even if it were to apply for a particular end point, such as cell transformation due to two specific chromosome deletions, it could only explain an RBE_M less than 2 for mammography X rays relative to conventional X rays. Higher values of RBE_M could be attained only at lower electron energies.

In the two-lesion model with threshold the RBE_M increases more than linearly with $f_\Delta(E)$. It remains to be seen whether the threshold can with this model explain a substantially larger RBE_M of 15 keV electrons. The analysis requires a modified version of the proximity function.

THE REDUCED PROXIMITY FUNCTION

As pointed out in the preceding section, only the track ends with energy Δ are taken to be effective in the threshold models. Accordingly, in the track simulations the energy cut-off is taken to equal the assumed threshold, Δ, for the lesion production. All other energy transfers are disregarded. The procedure implies that the track ends are treated as point events. This implies a loss of spatial resolution of about 3 nm for Δ = 100 eV, about 20 nm for Δ = 500 eV, and about 0.1 μm for 2 keV.

In the simulations the electron tracks are thus reduced to the track ends, Δ, alone (in the example of Fig. 1, the circles). All other energy transfers are disregarded. A *reduced proximity function*, $t_\Delta(x)$, is computed for the ''eroded'' tracks.

For small values of Δ, such as 100 eV, the reduced proximity function does not differ greatly from the familiar proximity function, except for the fact that the function is normalized[4] to $f_\Delta(E)^2 \cdot E$, rather than E. This normalization reflects the fact that the number of track ends—and of lesions—is for a specified radiation proportional to $f_\Delta(E)$. The square of $f_\Delta(E)$ enters the formulation, because of the assumed two-lesion process. It must be noted that, with this normalization, the expected energy due to track ends at distance x to $x + dx$ from a randomly selected track end is $t_\Delta(x)dx/f_\Delta(E)$, rather than $t_\Delta(x)dx$.

Numerical Results

In Fig. 2, the familiar proximity functions for 15 keV and 40 keV electron tracks have been plotted on a linear ordinate scale, which has the advantage that the area under a segment of the curve represents the expected energy within the corresponding distance interval. On the other hand, the effectiveness ratio, RBE_M, of two radiations equals under the two-lesion model the ratio of their proximity functions at the relevant distances, x. To show this ratio more clearly, and also for better readability of small ordinate values, the data are subsequently given in full logarithmic diagrams.

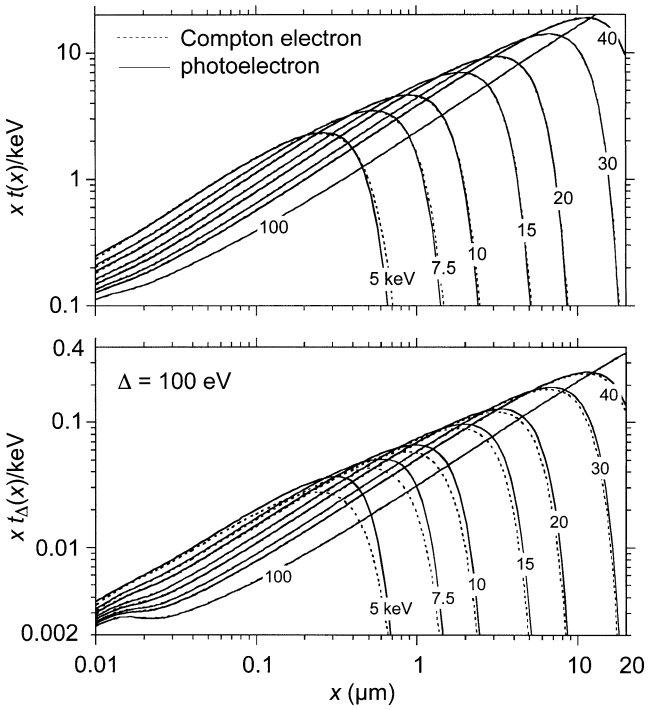

FIG. 4. Proximity functions (upper panel) and reduced proximity functions for Δ = 100 eV (lower panel) for specified electron energies. The solid curves correspond to photoelectrons, i.e. to tracks with an initial Auger electron; the broken curves correspond to Compton electrons.

The upper panel of Fig. 4 corresponds to Fig. 2; it gives the conventional proximity functions. The broken curves stand for Compton electrons, the almost coincident solid curves for photoelectrons.

The lower panel gives the reduced proximity functions for Δ = 100 eV. The curves for the photoelectrons lie, as expected, somewhat above those for the Compton electrons, but the difference is substantial only at low energies.

The values of RBE_M that correspond to these data will be considered in the subsequent section. But it has been pointed out already that the ratio of the proximity functions is the relevant parameter. The curves in Fig. 2 have suggested that—up to about 1 μm—the value is about 1.6 for 15 keV relative to 40 keV electrons. Figure 4 brings this out more clearly and shows that it applies equally with the assumed threshold Δ = 100 eV.

The data for Δ = 0.5 keV are given in Fig. 5. Here the values are substantially higher for the photoelectrons, which shows the significant impact that the initial Auger electron will have—especially at the lower electron energies—if a 0.5 keV threshold is assumed for the formation of lesions. The data for photoelectrons and Compton elec-

[4] The normalization of $t(x)$ includes at $x = 0$ a Dirac δ function $\varepsilon_w \delta(x)$, where ε_w equals Δ or the weighted mean of the energy transfers ε_i. This singularity at $x = 0$ is of no concern here, nor does it show in the graphic representations.

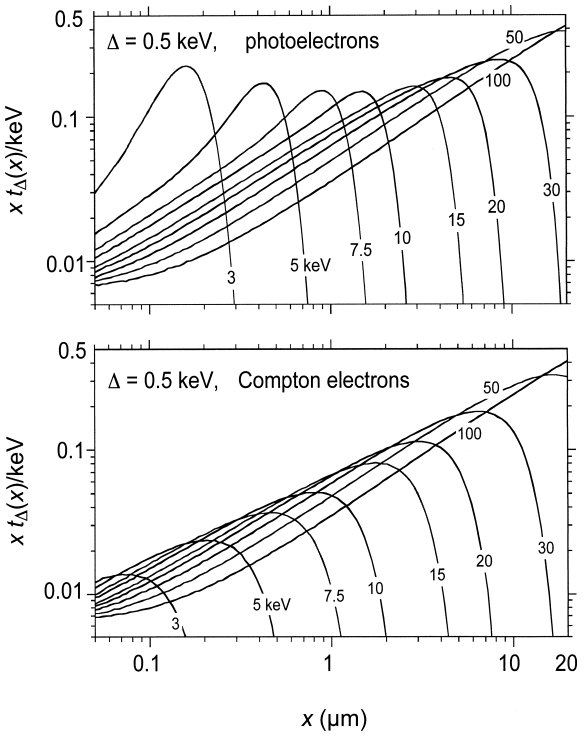

FIG. 5. Reduced proximity functions for $\Delta = 500$ eV. The upper panel gives the functions for photoelectrons. The lower panel gives the functions for Compton electrons (without an initial Auger electron).

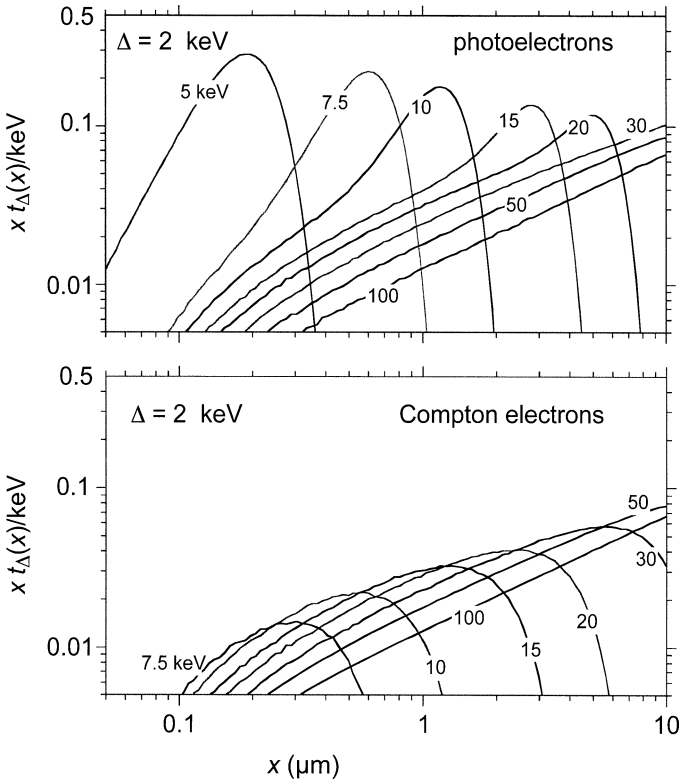

FIG. 6. Reduced proximity functions for $\Delta = 2$ keV. The upper panel gives the functions for photoelectrons, i.e. for tracks with an initial Auger electron (0.5 keV or 2 keV depending on photoelectric ionization cross sections). The lower panel gives the functions for Compton electrons (no initial Auger electron).

trons are markedly different and are therefore plotted separately.

The highly speculative 2 keV threshold model would attribute at low electron energies much of the effectiveness of the radiation to the roughly 15% of the Auger electrons that come from potassium, sulfur, phosphorus and chlorine in tissue and have higher energies. While the model is extreme, it is nevertheless of interest to contemplate its potential implications. As Fig. 6 shows, the influence of the more energetic Auger electrons is evidently very substantial in this case. It is only because of the occasional high-energy Auger electron at the origin of a 15 keV photoelectron that one 2 keV track end has a substantial chance to be accompanied by a second such track end within a distance of 1 to 4 μm.

RELATIVE BIOLOGICAL EFFECTIVENESS

Formula for RBE_M in the Two-Lesion Model

Rossi and Zaider (*11*) give—in terms of the familiar proximity function, $t(x)$—a useful survey of applications to radiobiology. A basic formula [(*11*); VI.49] expresses—for a two-lesion model—the initial linear component of the dose dependence as an integral over $t(x)$:

$$\alpha \propto \int \gamma(x)t(x)\,dx. \tag{4}$$

$\gamma(x)$ is the distance dependent *response function* that quantifies the probability that two lesions can be induced a distance x apart and can then combine (see Appendix for further explanation). Various studies have, for specific cellular end points, investigated the response function and, as expected, a decreasing function was inferred which reaches out to distances x of one or a few micrometers. However, in the present context there is no need to specify $\gamma(x)$. The essential point is that $\gamma(x)$ does not depend on the radiation, which implies, as will be seen, that significant conclusions on RBE_M can be obtained that apply irrespective of the response function.

The low-dose RBE of two radiations A and B equals the ratio of their linear dose coefficients:

$$RBE_M = \frac{\int \gamma(x)t_A(x)\,dx}{\int \gamma(x)t_B(x)\,dx}. \tag{5}$$

If the derivation of Eq. (4) is retraced, it is seen that the same relationship applies to models with threshold and the corresponding reduced proximity functions. The same formalism thus applies in both cases. Therefore, it is understood that in the equations $t(x)$ also stands for $t_\Delta(x)$.

Evidently the RBE_M of radiation A relative to radiation

B would be equal to the ratio $t_A(x)/t_B(x)$ of the proximity functions if a single distance x only or a narrow range of combination distances for lesions were relevant. Similarly, RBE_M equals the ratio $t_A(x)/t_B(x)$ if this ratio is constant over a broad range of distances. As can be seen from the data in Figs. 2 and 4, the ratio $t_{15keV}(x)/t_{40keV}(x)$ is roughly equal to 1.6 for distances up to about 1 μm. This confirms that the RBE_M of 15 keV electrons relative to 40 keV electrons will be about 1.6 if lesions can combine over distances up to about 1 μm. If larger distances play a role the ratio is less, and 1.6 is thus an upper bound for the RBE_M of 15 keV relative to 40 keV electrons. Inspection of the lower panel in Fig. 4 and of Fig. 5 shows that roughly the same conclusions apply in models with threshold 100 eV or 0.5 keV.

In a mathematically more concise form, one can state that no response function can make RBE_M in Eq. (5) larger than the maximum value of $t_A(x)/t_B(x)$. The statement uses the readily demonstrable fact that the ratio of two integrals over non-negative functions can never exceed the maximum ratio of the two functions. The maximum of the ratio of the proximity functions is thus an upper limit for the RBE_M of radiation A relative to radiation B.

Ratios of the Proximity Functions as Indicator of RBE_M Compared to 200 kV X Rays

The four panels in Fig. 7 represent, for photoelectrons of different energies and for the assumed threshold values, the ratio of their proximity function to that of 40 keV Compton electrons. The reference energy 40 keV is chosen, because it is close to the weighted mean electron energy, 36 keV, of 200 kV X rays with normal filtration (*2*). The diagrams in Fig. 7 correspond to the data in Figs. 4–6.

As has been confirmed in various studies, fairly high RBE_M values can be reached by low-energy electrons, e.g. electrons of 5 keV, if the relevant distances for the combination of lesions are fractions of a micrometer only.

The RBEs are less substantial at higher electron energies. The 15 keV photoelectrons are roughly representative for mammography radiation. They can, as has been concluded in the earlier sections, reach RBE_M values relative to 40 keV electrons of about 1.6. Since the ratio is about 1.6 at all distances up to about 1 μm, it is not merely an upper limit; i.e., the RBE_M will actually be close to 1.6 if lesions cannot combine over distances much larger than 1 μm. If a threshold $\Delta = 500$ eV is assumed for lesion formation, the value 1.6 can apply for the 15 keV electrons even if the relevant distances reach up to 2 or 3 μm.

With the high threshold 2 keV, the theoretical upper limit for the RBE_M of 15 keV electrons would actually be about 3. But this value could be attained only if lesions always combine over distances between 2 and 3 μm. This would require the assumption that two relevant targets—e.g. two chromosome sections that need to be deleted—are always spaced 2 to 3 μm apart, a possible but unlikely assumption.

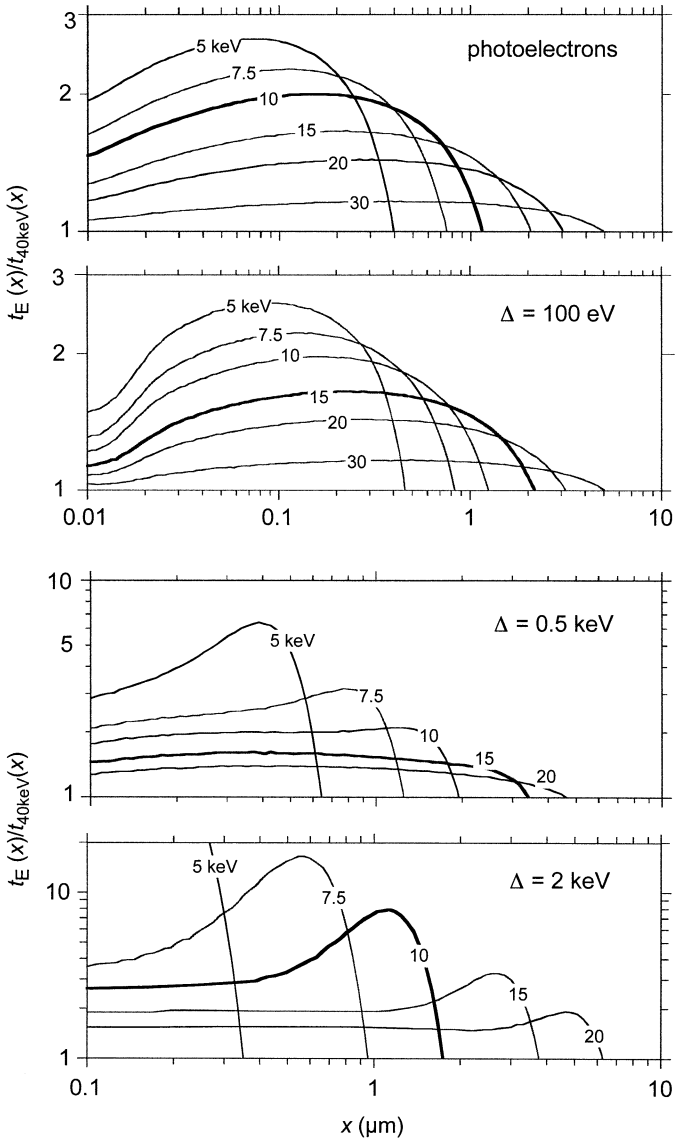

FIG. 7. The ratio of the proximity function for photoelectrons of specified energy to the proximity function of 40 keV Compton electrons. The 40 keV electrons correspond to the weighted mean electron energy from 200 kV X rays. The upper panel gives the familiar proximity functions which apply when no threshold is assumed for lesion induction. The three lower panels give the ratios for assumed thresholds of 100 eV, 500 eV and 2 keV. The peak value of each curve is an upper bound for the RBE_M of the electrons relative to 40 keV electrons. It would apply only if the corresponding x were the only relevant distance for the combination of two lesions.

In conclusion, a certain range effect, i.e. a correlation between critical interaction distance and the range of the most effective electrons, is seen in all models. But electron tracks have variable shape and range, and it is therefore not too surprising that for a given energy, such as 15 keV, the RBE_M varies remarkably little for assumed interaction distances up to 1 μm. In contrast to recent assumptions (*1, 2*) with this energy there is no distinct peak of RBE_M at interaction distances of a few micrometers. The only exception is—as discussed above—the highly speculative $\Delta = 2$

keV threshold model, and even there the peak between 2 and 3 μm is not, as seen in the lower panel of Fig. 7, very marked. There is thus no critical range effect, and the exploration in the earlier analysis (*3*) of a possible range effect of 10 keV to 20 keV electrons is seen to have been more than conservative.

CONCLUSIONS

In their treatment of the theory of dual radiation action (TDRA), i.e. radiation action through pairwise combination of lesions, Rossi and Zaider (*11*) discuss the possibility that it is not merely the combination of lesions that depends on radiation quality, but that the yield of the lesions itself can be dependent on radiation quality (*36, 37*). They speak in this context of *compound dual radiation action*:

> ''Other mechanisms that may be less obvious or unknown would also be subject to the formalism of *compound dual radiation action* if they involve lesions produced by highly localized energy absorption which combine in larger regions to form compound lesions. This interpretation requires major changes in the simple assumptions of the earliest forms of the *TDRA*'' (*11*).

The approach in terms of the reduced proximity function provides the required ''major change'' and still preserves the basic simplicity of the microdosimetric approach. It unifies the treatment of the various two-lesion interaction models of radiation action and extends it by incorporating the possibility of a threshold for lesion formation.

The computations have here been aimed at electron energies that are relevant to the RBE of mammography X rays relative to conventional X rays, and at the potentially greater effectiveness of photoelectrons in comparison to Compton electrons without an initial Auger electron. It is seen that photoelectrons can be substantially more effective at low energies than Compton electrons. However, a 15 keV photoelectron or one of higher energy will, together with its associated Auger electron, not be appreciably more effective than the Compton electron of the same total energy.

In the past, there has been—in spite of a number of informative applications—comparatively little use of the proximity function in radiobiological studies. One of the reasons may have been that the issue of RBE has been focused primarily on densely ionizing radiation, such as neutrons or heavy ions. For such radiations the differences in the microdosimetric parameters and the variations of RBE are so strongly pronounced that it is usually sufficient to use either measured microdosimetric spectra or computed spectra that disregard the complexities of δ-ray structure.

Recent attention to the RBE of different types of X rays and extensive new experimental studies with monoenergetic photons from synchrotron radiation have changed the situation. These new studies call for the exact treatment that can be performed in terms of the proximity function, including the use of the reduced proximity function to assess models with an assumed threshold for chromosomal lesions, such as breaks or deletions. The computational effort to derive the proximity functions used to be a major constraint, but this aspect has become less important. The microdosimetric analysis in terms of $t(x)$ or $t_\Delta(x)$ is thus fairly straightforward.

The major emphasis here has been on the two-lesion interaction process. This is not meant to imply that single-lesion action (*lesion–non-lesion interaction*) is of minor importance. In fact, the ultrasoft X-ray experiments (*17–19*) have demonstrated that single lesion action predominates at low electron energies; for higher energies its existence has recently been shown through experiments with cell fusion (*38*) or partial irradiation of the cell nucleus (*39*). However, as shown in terms of the *effective energy fraction* (see Fig. 3), single-lesion action cannot explain—regardless of the assumed threshold value, Δ—a high RBE of mammography X rays relative to conventional X rays. Accordingly, the analysis has been focused on the two-lesion process.

The threshold assumption has not been found to explain the high RBE values recently reported for mammography X rays compared to conventional X rays with regard to neoplastic transformations in human hybrid cells. The result of the present numerical treatment is thus in line with the assessment of the RBE_M of mammography X rays by Brenner and Amols (*8*) in terms of microdosimetric measurements (*40*). They are also consistent with new cell transformation data that Brenner *et al.* have obtained with 15 keV synchrotron radiation (*4*). The RBE could exceed 2 under the extreme assumption of the *''2 keV threshold two-deletion model''* where only the energy of the 2 keV track ends (including the higher-energy Auger electrons) is assumed to be effective, and where the distances between the two lesions are predominantly 2 μm and 3 μm. But even under these speculative assumptions, the RBE_M would not exceed a value of about 3.

The result of the analysis sharpens the conclusions of the preceding investigation (*3*) and confirms that the photo-induced Auger electrons are not a major factor at electron energies ≥15 keV. Under any realistic two-lesion model, 15 keV photoelectrons do not reach an RBE larger than about 1.6 relative to 40 keV electrons. The effective electron energy is larger than 15 keV for mammography X rays, but it is less than 40 keV for conventional 200 kV X rays (*3*). It follows that the RBE of mammography X rays relative to 200 kV X rays likewise will not exceed the value 1.6. An evaluation in terms of the actual proximity functions for mammography X rays and for 200 kV X rays might provide a slightly lower value of RBE, but it is unlikely to lead to markedly different conclusions.

APPENDIX: LINKAGE TO EARLIER MODELS

Rossi and Zaider have given a comprehensive treatment of microdosimetric tools for radiobiological analysis (*11*). This Appendix summarizes—in a somewhat more technical manner than the main part of the paper—the relationship of the present approach to the established concepts.

Earlier applications of microdosimetry to radiobiology employed predominantly measured data, namely *specific energy, z,* or lineal energy, *y,* in spherical microscopic sites of, say, diameter 1 μm. The analysis of a variety of radiobiological experiments, largely performed with neutrons, led to the conclusion that the cellular effects tend to be proportional to the square of the energy concentration in a critical site (*24*):

$$\mathcal{E}(z) = kz^2. \tag{A1}$$

It follows then from microdosimetric theory that at low doses the slope of the dose relationship is proportional to the dose mean specific energy per event, z_D:

$$\mathcal{E}(D) = \alpha D, \quad \text{with } \alpha = kz_D. \tag{A2}$$

This model, labeled dual action, can be interpreted in terms of the interaction of pairs of lesions produced in sensitive sites—typically of dimension 1 μm or less—in the cell.

A fundamental relationship links the dose mean specific energy, z_D, to the proximity function, $t(x)$, and the geometric reduction factor, $U(x)$, of the site[5] (*10, 11, 26*):

$$z_D = \int t(x)U(x)/m \quad (m\text{: mass of the site}). \tag{A3}$$

With the assumption in Eq. (A2), the low-dose relative biological effectiveness of two radiations, A and B, is therefore:

$$\mathrm{RBE_M} = \frac{\int t_{\Delta,A}(x)U(x)\,dx}{\int t_{\Delta,B}(x)U(x)\,dx}. \tag{A4}$$

In a more general interpretation (*25*), $U(x)$ has been replaced by a function $\gamma(x)$ that incorporates in addition a distance-dependent lesion interaction probability, $g(x)$:

$$\gamma(x) \propto U(x)g(x). \tag{A5}$$

Equation (A4) was used in this form—i.e. as in Eq. (5)—for the determination of interaction distances in the molecular ion-beam experiments (*36, 37*) and in subsequent studies (*12–14*). The geometric reduction factor for a sphere of diameter d is (*10, 41*)

$$U(x) = 1 - 3x/2d + x^3/2d^3. \tag{A6}$$

A plausible form of the distance dependent interaction probability is

$$g(x) \sim \exp[-(x/\delta x)] \quad (\delta x\text{: effective interaction distance}). \tag{A7}$$

Figure A1 represents special cases of the resulting response function $\gamma(x)$. The solid curves correspond to the assumption of a spherical site and a distance-independent combination probability of lesions [$g(x) = \text{const}$]. The dotted lines give the functions, $\gamma(x)$, that result if, in addition, the distance-dependent interaction probability, $g(x)$, is included.

The left solid curve relates to a spherical site with 1 μm diameter, which corresponds to common microdosimetric measurements. It is apparent from this graph that the relevant distributions, $\gamma(x)$, can have similar shape, regardless of whether the interaction is constrained by the dimension of the spherical region alone (solid curves) or jointly by the two factors (dotted curves). Lesion interaction with effective interaction distance 0.4 μm within a large site is roughly equivalent to distance independent interaction in a site of 1 μm diameter.

Microdosimetric measurements, although related to a spherical volume, with no accounting for a distance-dependent interaction probability, are therefore also adequately representative for the more realistic case of lesions interacting in the larger nuclear matrix of the cell (*25*).

[5] If P is a random point in a site S, the geometric reduction factor $U(x)$ equals the probability that a point at a distance x in random direction from P is contained in S. The point-pair distance distribution of S is closely related to $U(x)$ (*41*).

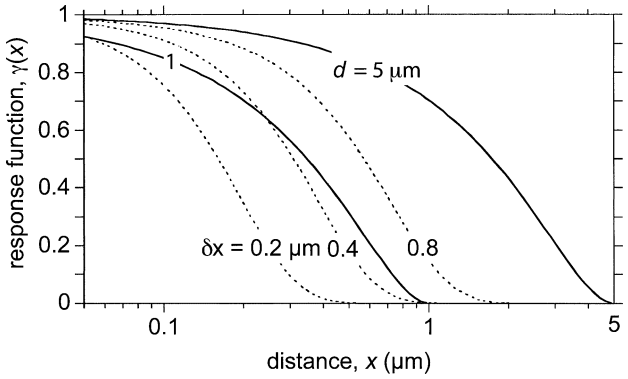

FIG. A1. The response function $\gamma(x)$ under typical assumptions. The solid lines result if lesions are produced within a spherical site of diameter 1 or 5 μm, and all pairs are equally likely to combine. The dotted lines are the result for a spherical site (5 μm) with distance-dependent interaction probability and effective interaction distance δx = 0.2, 0.4, and 0.8 μm (see Eq. A7).

For any two electron energies ≥15 keV, the ratio of the proximity functions is almost constant from fractions of a micrometer to about 1 μm; i.e., there is little change with distance in the ratios of the proximity functions (see Figs. 4–6). This implies that Eq. (5), i.e. the generalization of Eq. (A4), can be approximated by the ratio of the proximity functions in terms of one representative distance.

It is apparent that the equations can be modified by substituting the reduced proximity function, $t_\Delta(x)$, for the conventional proximity function, $t(x)$. The minor impact of the threshold assumption on the results for ≥15 keV (see Figs. 4 and 5) attests to the relative insensitivity of microdosimetric measurements with photon or electron radiations to factors such as the ionization yield or the characteristics of the counter gas.

Received: August 26, 2002; accepted: April 9, 2003

REFERENCES

1. D. Frankenberg, K. Kelnhofer, K. Bär and M. Frankenberg-Schwager, Mammographie-Röntgenstrahlen sind für die neoplastische Transformation einer menschlichen Hybridzelllinie um den Faktor 3,4 effektiver als 200kVp-Röntgenstrahlen. *Strahlenbiologie und Strahlenschutz*, Band I, 27–40 (2000).
2. D. Frankenberg, K. Kelnhofer, K. Bär and M. Frankenberg-Schwager, Enhanced neoplastic transformation by mammography X rays relative to 200 kVp, X rays: Indication for a strong dependence on photon energy of the $\mathrm{RBE_M}$ for various end points. *Radiat. Res.* **157**, 99–105 (2002).
3. A. M. Kellerer, Electron spectra and the RBE of X rays. *Radiat. Res.* **158**, 13–22 (2002).
4. D. J. Brenner, S. G. Sawant, M. P. Hande, R. C. Miller, C. D. Elliston, Z. Fu, G. Randers-Pehrson and S. A. Marino, Routine screening mammography: How important is the radiation-risk side of the benefit-risk equation. *Int. J. Radiat. Biol.* **78**, 1065–1067 (2002).
5. E. Schmid, Is there reliable experimental evidence for low dose RBE of about 4 of mammography X rays relative to 200kV X rays? *Radiat. Res.* **158**, 778–781 (2002). [commentary]
6. M. S. Sasaki, K. Kobayashi, K. Hieda, T. Yamada, Y. Ejimat, H. Maezawa, T. Furusawa, T. Ito and S. Okada, Induction of chromosome aberrations in human lymphocytes by monochromatic X rays of quantum energy between 4.8 and 14.6 keV. *Int. J. Radiat. Biol.* **56**, 975–988 (1989).
7. E. Schmid, D. Regulla, H. M. Kramer and D. Harder, The effect of 29 kV X rays on the dose response of chromosome aberrations in human lymphocytes. *Radiat. Res.* **158**, 771–777 (2002).
8. D. J. Brenner and H. I. Amols, Enhanced risk from low-energy

screen-film mammography X rays. *Br. J. Radiol.* **62**, 910–914 (1989).

9. D. Harder, R. Greinert and D. Frankenberg, Characteristics of electron tracks in matter. In *Radiation Research*, Vol. 2 (M. Moriarty, C. Mothersill, C. Seymour, M. Edington, J. F. Ward and R. J. M. Fry, Eds.), pp. 111–114. Allen Press, Lawrence, KS, 2000.
10. A. M. Kellerer and D. Chmelevsky, Concepts of microdosimetry. III. Mean values of the microdosimetric distributions. *Radiat. Environ. Biophys.* **12**, 321–335 (1975).
11. H. H. Rossi and M. Zaider, *Microdosimetry and Its Applications.* Springer, Heidelberg, 1996.
12. C. S. Wuu and M. Zaider, A calculation of the relative biological effectiveness of ^{125}I and ^{103}Pd brachytherapy sources using the concept of proximity function. *Med. Phys.* **25**, 2186–2189 (1998).
13. R. Taschereau, R. Roy and J. Pouliot, Relative biological effectiveness enhancement of a ^{125}I brachytherapy seed with characteristic X rays from its constitutive materials. *Med. Phys.* **29**, 1397–1402 (2002).
14. M. Zaider and D. J. Brenner, On the stochastic treatment of fast chemical reactions. *Radiat. Res.* **100**, 245–256 (1984).
15. D. Chmelevsky and A. M. Kellerer, Proximity functions for electrons up to 10 keV. *Radiat. Res.* **84**, 219–238 (1980).
16. ICRU, *Microdosimetry.* Report 36, International Commission on Radiation Units and Measurements, Bethesda, MD, 1983.
17. R. Cox, J. Thacker and D. T. Goodhead, Inactivation and mutation of cultured mammalian cells by aluminum characteristic ultrasoft X-rays II. Dose-responses of Chinese hamster and human diploid cells to aluminum X-rays and radiations of different LET. *Int. J. Radiat. Biol.* **31**, 561–576 (1977).
18. D. T. Goodhead, Inactivation and mutation of cultured mammalian cells by aluminum characteristic ultrasoft X-rays III. Implication for theory of dual radiation action. *Int. J. Radiat. Biol.* **32**, 43–70 (1977).
19. D. T. Goodhead and D. J. Brenner, The mechanism of radiation action and the physical nature of biological lesions. In *Radiation Protection*, Proceedings on the Eighth Symposium on Microdosimetry (J. Booz and H. G. Ebert, Eds.), pp. 597–609. Report EUR 8395 En, Commission of the European Communities, Luxembourg, 1982.
20. M. Zaider, D. Brenner and W. E. Wilson, The applications of track calculations to radiobiology. I. Monte-Carlo simulation of proton tracks. *Radiat. Res.* **95**, 231–247 (1983).
21. A. M. Kellerer, K. Hahn and H. H. Rossi, Intermediate dosimetric quantities. *Radiat. Res.* **130**, 15–25 (1992).
22. W. E. Moddeman, T. A. Carlson, M. O. Frause, B. P. Pullen, W. E. Bull and G. K. Schweizer, Determination of the K-LL Auger spectra of N_2, O_2, CO, NO, H_2O and CO_2. *J. Chem. Phys.* **55**, 2317–2336 (1971).
23. J. Chen, E. Nekolla and A. M. Kellerer, A comparative study of microdosimetric properties of X-rays, γ-rays, and β-rays. *Radiat. Environ. Biophys.* **35**, 263–266 (1996).
24. A. M. Kellerer and H. H. Rossi, The theory of dual radiation action. *Curr. Top. Radiat. Res. Q.* **8**, 85–158 (1972).
25. A. M. Kellerer and H. H. Rossi, A generalized formulation of dual radiation action. *Radiat. Res.* **75**, 471–488 (1978).
26. A. M. Kellerer, Fundamentals of microdosimetry. In *The Dosimetry of Ionizing Radiation*, Vol. 1, pp. 77–162. Academic Press, San Diego, 1985.
27. D. E. Lea, *Action of Radiations on Living Cells.* Cambridge University Press, Cambridge, 1946.
28. S. Wolff, In *Repair from Genetic Damage* (F. Sobels, Ed.), pp. 1–10. Pergamon Press, 1963.
29. W. M. J. Veigele, Photon cross sections from 0.1 keV to 1 MeV for elements Z = 1 to Z = 94. *At. Data* **5**, 51–111 (1973).
30. ICRU, *Tissue Substitutes in Radiation Dosimetry and Measurement.* Report 44, International Commission on Radiation Units and Measurements, Bethesda, MD, 1989.
31. S. Saigusa, Y. Ejima, K. Kobayashi and M. S. Sasaki, Induction of chromosome aberrations by monochromatic X-rays with resonance energy of phosphorus K-shell absorption edge. *Int. J. Radiat. Biol.* **61**, 785–790 (1990).
32. D. Harder and R. Greinert, Vibrational energy relaxation—a proposed pathway of fast local chromatin denaturation. *Radiat. Prot. Dosim.* **99**, 183–188 (2002).
33. M. S. Mendonca, K. Howard, C. L. Fasching, D. L. Farrington, E. J. Desmond, E. J. Stanbridge and J. L. Redpath, Loss of suppressor location chromosomes 11 and 14 may be required for radiation-induced neoplastic transformation of HeLa skin fibroblast human cell hybrids. *Radiat. Res.* **149**, 246–255 (1998).
34. V. L. Spencer and U. Fano, *Phys. Rev.* **93**, 1172 (1954).
35. H. G. Paretzke, An appraisal of the relative importance for radiobiology of effects of slow electrons. In *Proceedings of the Fifth Symposium on Microdosimetry* (J. Booz, H. G. Ebert and B. G. R. Smith, Eds.). Commission of the European Communities, Brussels, 1976.
36. H. H. Rossi, Biophysical studies with spatially correlated ions. 1. Background and theoretical considerations. *Radiat. Res.* **78**, 185–191 (1979).
37. A. M. Kellerer, Y. M. P. Lam and H. H. Rossi, Biophysical studies with spatially correlated ions. 4. Analysis of cell survival data for diatomic deuterium. *Radiat. Res.* **83**, 511–528 (1980).
38. F. Darroudi, A. T. Natarajan, J. R. K. Savage and D. Harder, Induction of chromosomal aberrations by low and high LET radiations: Mechanisms and spectra. In *European Radiation Research 2001*, Proceedings of 31st Annual Meeting of the European Society for Radiation Biology (ESRB) (W. Dorr, D. Frankenberg, D. Harder and K. Kiefer, Eds.). Dresden, 2001.
39. G. Ludwikow, Y. Xiao, R. A. Hoebe, N. A. P. Franken, F. Stap, C. H. Van Oven, C. J. F. Van Noorden and J. A. Aten, Induction of chromosome aberrations in unirradiated chromatin after partial irradiation of a cell nucleus. *Int. J. Radiat. Biol.* **78**, 239–247 (2002).
40. R. Dvorak and P. Kliauga, Microdosimetric measurements of ionization by monoenergetic photons. *Radiat. Res.* **73**, 1–20 (1978).
41. A. M. Kellerer, Chord-length distributions and related quantities for spheroids. *Radiat. Res.* **98**, 425–437 (1984).